analytical chemistry

pubs.acs.org/ac Article

Single Molecule Kinetic Fingerprinting of Glycans on IgA1 Antibodies

Joseph R. Rubin, Steven K. Taylor, Sergei Rudchenko, Milan N. Stojanovic, and Henry Hess*

Cite This: *Anal. Chem.* 2025, 97, 14388−14396 Read Online

ACCESS | Metrics & More | Article Recommendations | Supporting Information

ABSTRACT: Immunoglobulin A (IgA) nephropathy is the most common form of primary glomerulonephritis and is triggered by damage to glomeruli from deposition of complexes formed between glycosylated IgA1 antibodies that are "galactose-deficient" and antibodies directed to these aberrant proteins. Currently, galactose deficiencies are detected with ensemble measurements, e.g., via mass spectrometry or liquid chromatography, which only measure average glycan-IgA1 ratios, but cannot resolve heterogeneity of O-glycosylation between different IgA1 populations. To resolve these differences at the single molecule level, we developed an assay to detect the glycosylation state of individual IgA1 using single molecule fluorescence microscopy. By using fluorescence resonance energy transfer (FRET), high concentrations of fluorescently labeled probes with low binding rates can be employed to observe the binding of protein probes to surface adhered target molecules and obtain their kinetic fingerprints. We measured the binding and unbinding rates of jacalin (a lectin binding to O-linked glycans) to individual IgA1 molecules on a glass surface. Adding galactose decreased binding, which demonstrated that the jacalin probe binds specifically to O-linked glycans on the hinge region of IgA1. This result is a first step toward using kinetic fingerprinting to sequence glycans on IgA1.

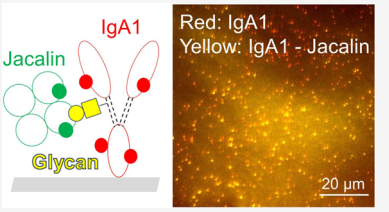

INTRODUCTION

IgA nephropathy (IGAN) is the most common form of primary glomerulonephritis.[1,2] The disease is triggered by the damage to glomeruli from deposition of complexes formed between polyclonal IgA1 antibody proteins that are "galactose-deficient" (GD-IgA1) and antibodies directed to these GD-IgA1.[1−3] Currently, galactose deficiencies are detected through mass spectrometry, liquid chromatography, immunoblotting, and other ensemble methods.[4,5] Ensemble measurements, however, only measure average glycan-IgA1 ratios, but cannot resolve heterogeneity of O-glycosylation between different IgA1 populations. Even when mass spectrometry is combined with protein fractionation,[6] quantifying glycans on both IgA1 hinges simultaneously remains challenging. To resolve heterogeneity in O-glycosylation, we aim to develop an assay to detect GD-IgA1 using single molecule fluorescence measurements.

Single molecule localization microscopy (SMLM) techniques overcome the diffraction limit by imaging dispersed fluorophores and deducing their location with nanometer accuracy.[7,8] SMLM techniques include fluorescence photoactivated localization microscopy (PALM),[9−12] in which dyes are turned on and off through illumination; stochastic optical reconstruction microscopy (STORM),[13] in which dyes are turned on and off through varying buffer conditions or dyes which spontaneously blink; and point accumulation for imaging in nanoscale topography (PAINT),[7,14,15] in which labeled probes temporarily bind to the analyte. Due to constant replenishment of the probe from solution, PAINT overcomes limitations caused by photobleaching,[15] such as a limit on the number of photons which can be collected from an individual molecule. PAINT not only allows for the more precise localization of independent molecules, but also allows for the characterization of additional properties of the molecules, such as the binding and unbinding rates of the probes to the molecules.[15] The binding and unbinding rates of one or more probes to a single target molecule constitute a kinetic fingerprint specific to that molecule.

Single molecule kinetic fingerprinting can, in principle, detect GD-IgA1 using lectin probes. Lectins are nonimmune proteins that bind specifically to carbohydrates.[16] Kinetic fingerprinting using lectins, however, is challenging due to their low binding affinity relative to traditional probes for fingerprinting, such as nucleic acids and antibody fragments.[15,17−21] These more common probes have on-rates on the order of 10^6 to 10^7 M^{-1} s^{-1}, which have been even further accelerated to 8×10^7 M^{-1} s^{-1} in a method termed protein-assisted DNA-PAINT.[22] This means that with a probe concentration of 100 nM, one can observe on average one binding event per analyte molecule within seconds. Lectins, on the other hand, often have on-rates on the order of 10^3 to 10^5 M^{-1} s^{-1}.[23,24] This hundred-fold lower on-rate dramatically reduces the number of

Received: March 11, 2025
Revised: June 4, 2025
Accepted: June 25, 2025
Published: July 2, 2025

https://doi.org/10.1021/acs.analchem.5c01488
Anal. Chem. 2025, 97, 14388−14396

observable events, unless the probe concentration is increased. Higher concentrations of the fluorescently labeled probe lead to proportionally higher levels of background fluorescence, both due to protein probes in solution and to nonspecific binding of the protein probes to the substrate. The issue of background from probes in solution has been addressed in the context of DNA point accumulation for imaging in nanoscale topography (DNA-PAINT) by the use of single molecule fluorescence resonance energy transfer (smFRET).[25] smFRET is a fluorescence resonance energy transfer technique in which a single fluorescently labeled donor molecule excites a single fluorescently labeled acceptor molecule.[26−31] SmFRET has also been applied to observe conformational changes within a protein,[26,27] to track movement of ions in anisotropic polyelectrolyte multilayers,[32] to measure the binding kinetics of cadherins tethered to membranes,[33] and to measure interactions of proteins confined to vesicles.[34,35] Single molecule FRET has even been used in conjunction with DNA probes to detect amino acids and glycans on full length proteins.[36] Utilizing unconfined protein probes, however, remains a challenge because proteins bind nonspecifically much more readily to a glass surface than DNA and blocking the surface completely is nearly impossible.[37−40] A method termed resPAINT (reservoir PAINT) decreases the background by utilizing photoactivatable or blinking protein probes,[41] which enables localization but not necessarily single molecule kinetic fingerprinting. SmFRET can potentially reduce the background arising from protein probes, because only probes located within a few nanometers of the target molecule contribute to fluorescence in the acceptor channel.

This work investigates if FRET PAINT can be used to observe the binding of protein probes to surface adhered molecules and obtain their kinetic fingerprints. We measured the binding and unbinding rates of jacalin (a lectin binding to O-linked glycans) to individual IgA1 molecules adhered on a surface (Figure 1a). The specificity of the observed binding events was confirmed by adding D-galactose. Based on the surface plasmon resonance experiments on α methyl galactose of Smith et al.[42] and the bulk agglutination experiments comparing α methyl galactose and D-galactose binding jacalin of Hagiwara et al.,[43] D-galactose binds to the jacalin probes with a K_D < 1 mM, thus it will block jacalin from binding specifically to O-linked glycans on the hinge region of IgA1 if present at mM concentrations. This negative control confirms that the jacalin probe can be used to detect the O-linked Glycans. This result is a first step toward kinetically fingerprinting posttranslational modifications of individual proteins.

MATERIALS AND METHODS

Jacalin (L-1150−25, Vector Laboratories) was labeled with CY3 (PA13101, Cytiva) and Human IgA1 (Cell Sciences, CSI19836B) was labeled with Alexa Fluor 647 (A20006, Fisher) by conjugation to primary amines via NHS linkers. The labeling ratio was 5.5 fluorophore molecules per jacalin tetramer and 5 fluorophore molecules per IgA1 monomer, as determined by measuring absorbance with a Nanodrop 1000 UV/vis spectrophotometer at 280 nm for proteins, and at 552 and 650 nm for CY3 and Alexa Fluor 647, respectively. The brightness distributions of our data are consistent with the expected Poisson distribution (Figure S12).[44] No. 1 borosilicate glass coverslips (1419−10, Globe Scientific) were cleaned by rinsing thrice with ultrapure water, sonication

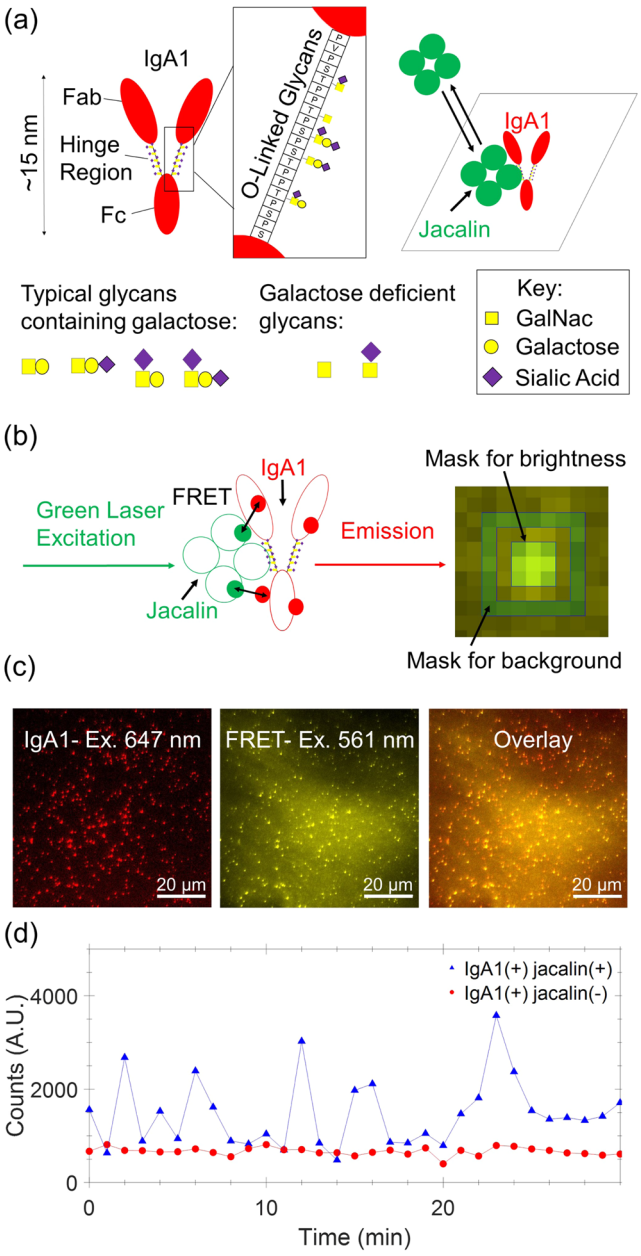

Figure 1. (a) Jacalin in solution can temporarily bind to glycans linked to IgA1 molecules physisorbed to a glass substrate. (b) The binding is detected by FRET imaging and the intensity of each spot is determined by subtracting the background from the integrated brightness. (c) Images from the flow cell of adsorbed IgA1 in the presence of 800 nM jacalin. The positions of the Alexa647-labeled IgA1 molecules can be identified by excitation with 647 nm light. The locations of bound Cy3-labeled jacalin molecules can be determined by FRET imaging (excitation with 561 nm light). In the overlay, unoccupied IgA1 appears red and occupied IgA1 appears yellow. (d) FRET time trace for an IgA1 spot when jacalin (800 nM) is present in the solution compared to a trace with similar IgA1 brightness when jacalin is absent.

in ultrapure water for 5 min, in acetone for 20 min, in 1 M potassium hydroxide for 20 min, and finally in ultrapure water for 20 min, with thrice rinsing with ultrapure water repeated after each sonication step. The coverslips were dried in an oven or by blowing nitrogen gas over them. Finally, the coverslips were plasma cleaned in a UV-ozone cleaner for at least 20 min

https://doi.org/10.1021/acs.analchem.5c01488
Anal. Chem. 2025, 97, 14388−14396

prior to experiments. Flow cells were created by sticking circular perfusion chambers (622505, Grace Bio-Labs; 38 μL volume; 8−9 mm diameter; 0.6 mm depth; 1.5 mm diameter ports) to the cleaned coverslips.

A solution of 300 pM labeled IgA1 in HBS (HEPES-buffered saline, 10 mM 2-[4-(2-hydroxyethyl)piperazin-1-yl]ethane-1-sulfonic acid, 150 mM NaCl, 1 mM $CaCl_2$, pH = 7.5) was infused into the flow cell for 10 min to physisorb IgA1 to the glass coverslip. The perfusion chambers were subsequently rinsed twice with HBS and once with 27 mg/mL Blocking Reagent for Elisa (11112589001, Sigma) in HBS; each rinse consisted of 38 μL of solution, with old solution being removed by absorbing it with a kimwipe on one side while simultaneously pipetting in new solution on the other side. Next, a solution consisting of 0−800 nM labeled jacalin; 27 mg/mL Blocking Reagent for Elisa; an oxygen scavenging system consisting of 40 mM glucose (G7258−250G, Sigma), 9 U/mL pyranose oxidase (P4234−250UN, Sigma; PYR-Z-E11, United Immunoassay), and 0.008 mg/mL catalase (C40−500MG, Sigma); triplet quenchers which include 4 mM Trolox (238813−1G, Sigma), 3 mM 4-nitrobenzyl alcohol (N12821−25G, Sigma), and 3 mM cyclooctatetraene (138924−1G, Sigma); and 0−500 mM D-(+)-galactose (G0750−10G, Sigma) in HBS was flowed in (imaging solution was adapted from Usaj et al.[45]). The coverslip surface was imaged on a Nikon TiE epi-fluorescence microscope with a 100× oil objective (NA = 1.49) with an electron-multiplying charge-coupled device (EMCCD) camera (iXON DU897, Andor).

For the FRET channel, corresponding to jacalin binding to IgA1, the sample was illuminated once every minute by a 100 mW Sapphire 561 nm laser (Sapphire 561 LP, Coherent) with the laser power set to 50% for 5 s with an equivalent exposure time. A 561 nm filter cube (ZET561/10x EX, ZT561rdc BS, ET575lp EM, Chroma) was used with an additional emission filter (ET 700−75 bandpass, Chroma) to block donor emission. For the acceptor channel, corresponding to all IgA1 on the surface, the sample was illuminated by a 140 mW 647 nm laser (PhoxX 647, Omicron), with the laser power set to 4% with an exposure time of 300 ms, at the beginning of the video and once every 30 min. A 488/640 nm dual filter cube (ZET488/640x EX, ZT488/640rpc BS, ZET488/640m-TRF EM, Chroma) with the additional emission filter (ET 700−75 bandpass, Chroma) was used.

For each of the videos, the first hour was analyzed (61 frames), except for the control without jacalin, which only ran for the duration to acquire two IgA1 images which allows the analysis of 30 min of data in-between (31 frames).

The analysis was performed using ImageJ and custom Matlab (The Mathworks, Inc., Natick, MA) code. IgA1 molecules were chosen manually in ImageJ with Fiji.[46] Details of the generation of time traces can be found in the Supporting Information. Briefly, drift correction was done using Picasso software.[47] After drift correction, for each IgA1 location, the brightest pixel within a 2-pixel radius was automatically identified and the intensity of this pixel and its neighbors was summed after the local background intensity (defined by the average of the 24 outer pixels surrounding the brightest pixel in a square with side length 7) was subtracted, yielding brightness traces of single molecules over time. The mask method of measuring the brightness of each spot has an excellent correlation with the fitting of a Gaussian but without the computational demand (although the numerical brightness values of the Gaussian are twice as large). These single molecule time traces were generated for both the acceptor channel and the FRET channel.

In the acceptor channel, to analyze in a given trace how long IgA1 was present before leaving or acceptor photobleaching, time traces were compared to spots on the surface without IgA1 present. 160 random spots without IgA1 present in the 800 nM jacalin video were chosen, and the average brightness plus 4 standard deviations was used as the threshold for IgA1 photobleaching or leaving (Figure S4). All time points in a given trace after the IgA1 brightness dipped below this threshold due to photobleaching or loss of IgA1 were considered as of no interest and removed, as well as any frames in the FRET channel after the last frame in which the acceptor was above the threshold.

After correcting for acceptor absence, each FRET channel trace was divided by the average value of the first 2−3 frames of the acceptor channel trace, to correct for both variations in the illumination due to the laser profile and variations in the number of acceptor dyes attached to each IgA1 molecule. After this correction, traces were thresholded based on the mean of the control without jacalin plus 3 standard deviations to obtain kinetic rates (see Supporting Information).

For each IgA1 molecule, we calculated the kinetic binding rates and unbinding rates (also called off-rates) under the assumption that the bright-times and dark-times are exponentially distributed (as in the experiments of Kastantin et al.[48]). Therefore, if the probe is present in one frame at molecule index i, the probability that the probe is also present at that same molecule in the next frame is

$$p_{\mathrm{bound},i}(t_{n+1}|t_n) = \mathrm{e}^{-k_{\mathrm{off},i}\Delta t}$$

where $k_{\mathrm{off},i}$ is the unbinding rate for IgA1 molecule i and Δt is the time interval between frames.

Similarly, the probability that a probe does not bind to molecule i in a frame when it was not bound to molecule i in the previous frame is

$$p_{\overline{\mathrm{bound}},i}(t_{n+1}|t_n) = \mathrm{e}^{-\tau_{\mathrm{dark},i}{}^{-1}\Delta t}$$

where $\tau_{\mathrm{dark},i}{}^{-1}$ is the concentration-dependent observed binding rate (here on referred to as binding rate) for IgA1 molecule i. The binding rates and unbinding rates were therefore determined as follows

$$\tau_{\mathrm{dark},i}{}^{-1} = -\ln\left(\frac{n_{d,t,t+1,\mathrm{i}}}{n_{d,t,i}}\right)$$

$$k_{\mathrm{off},i} = -\ln\left(\frac{n_{b,t,t+1,\mathrm{i}}}{n_{b,t,i}}\right)$$

where $n_{d,t,t+1,i}$ is defined as the number of frames in which the probe is absent from IgA1 molecule i in both that frame and the following frame; $n_{d,t,i}$ is defined as the total number of frames in which the probe is absent from molecule i (excluding the last frame); $n_{b,t,t+1,i}$ is defined as the number of frames in which the probe is bound to IgA1 molecule i in both that frame and the following frame; and $n_{b,t,i}$ is defined as the total number of frames in which the probe is bound to IgA1 molecule i (excluding the last frame).

To define the ensemble apparent binding and unbinding rates in each experiment, the median of the binding and unbinding rates of the observed IgA1 molecules was

https://doi.org/10.1021/acs.analchem.5c01488
Anal. Chem. 2025, 97, 14388−14396

Table 1. Number of IgA1 at Each Analysis Stage for Different Jacalin and Galactose Concentrations

stage	80 nM jacalin	400 nM jacalin	800 nM jacalin	800 nM jac 5 mM gal	800 nM jac 50 mM gal	800 nM jac 500 mM gal	0 nM jacalin
total nonoverlapping IgA1	94	200	153	169	143	237	406
number remaining after 30 min	36	91	83	78	77	142	360
number remaining after 30 min and never bright	15	6	3	12	35	77	346
number remaining after 30 min and never dark	0	15	20	7	5	7	2
number remaining after 30 min and containing bright and dark frames	21	70	60	59	37	58	16
number used for calculating median binding rates	21	65	51	54	33	52	0
number used for calculating median unbinding rates	12	55	55	45	24	31	0
number used for calculating dissociation constants	12	50	48	41	20	27	0

determined, and the 95% confidence intervals were calculated using the bootstrap method. Box plots and jitter plots were generated by externally sourced Matlab code.[49]

To account for overlapping binding events and nonspecific binding, Monte Carlo simulations were run using both the 1-site and the 2-site binding model (see Supporting Information). 300 traces were simulated using parameters based on the experimental data, and the median with the 95% confidence intervals was plotted and compared to the experimental values.

RESULTS AND DISCUSSION

In our experiments, we physisorbed 300 pM IgA1 labeled with Alexa Fluor 647 (in the following referred to as the acceptor) to a cleaned glass coverslip surface, washed out the unbound IgA1 with buffer, exposed the surface to blocking reagent, and introduced a solution of jacalin labeled with CY3 (the donor) at concentrations 80, 400, and 800 nM to the flow cell. The physisorbed IgA1 molecules appear as several hundred isolated bright spots in the acceptor emission channel when TIRF-excited with a 647 nm laser (Figure 1c left, false colored red). Jacalin molecules binding to the IgA1 molecules cannot be directly imaged by TIRF-exciting with a 561 nm laser and collecting their emission in the donor channel due to the high background and the presence of particles even in the absence of IgA1 (Figure S1). We attribute a part of the background to nonspecific binding of jacalin molecules to the surface and the particles to aggregates on the surface despite the blocking. However, Jacalin molecules binding to the IgA1 molecules can be observed by FRET imaging, where the surface is TIRF-illuminated with a 561 nm laser to excite the donor fluorophores on the jacalin and the emission is observed in the acceptor channel (Figure 1c center, FRET imaging, false colored green). Since the acceptor is weakly excited by the 561 nm laser, IgA1 molecules without a donor nearby appear as dim spots, whereas IgA1 molecules with Jacalin molecules in their immediate vicinity appear brighter (Figure S2). Overlaying the two images yields an image (Figure 1c right) revealing the position of IgA1 molecules that colocalize with brighter particles in the FRET channel (yellow) and IgA1 that do not colocalize with brighter particles in the FRET channel (red).

IgA1 spots were picked by hand. Roughly half of these spots remained after 30 min, and only those that remained were used to determine the binding kinetics (Table 1). To calculate the brightness of IgA1 and colocalized spots in the FRET channel, the intensity of the brightest pixel and its neighbors was summed after the local background intensity was subtracted, yielding brightness traces of single molecules over time (Figure 1d), as described in the Supporting Information. To avoid overlap of the mask for the background overlapping with adjacent particles, only IgA1 spots outside of 6 pixels of each other were chosen.

The brightness of the IgA1 molecules when excited directly with 647 nm light varied widely due to their varying number of acceptor dyes and their exposure to varying excitation intensities (Figure 2a). The weaker excitation with 561 nm light leads to a roughly proportional variability in detected brightness, but with a reduced average magnitude. In the presence of 800 nM jacalin, the brightness (and its variability) of the spots when excited with 561 nm light greatly increases. Dividing the brightness of each spot when excited with 561 nm light (its FRET brightness) by its brightness when excited with 647 nm light effectively removes the variability of the signal due to variations in excitation intensity and variations in the number of acceptor dyes at each IgA1 location.

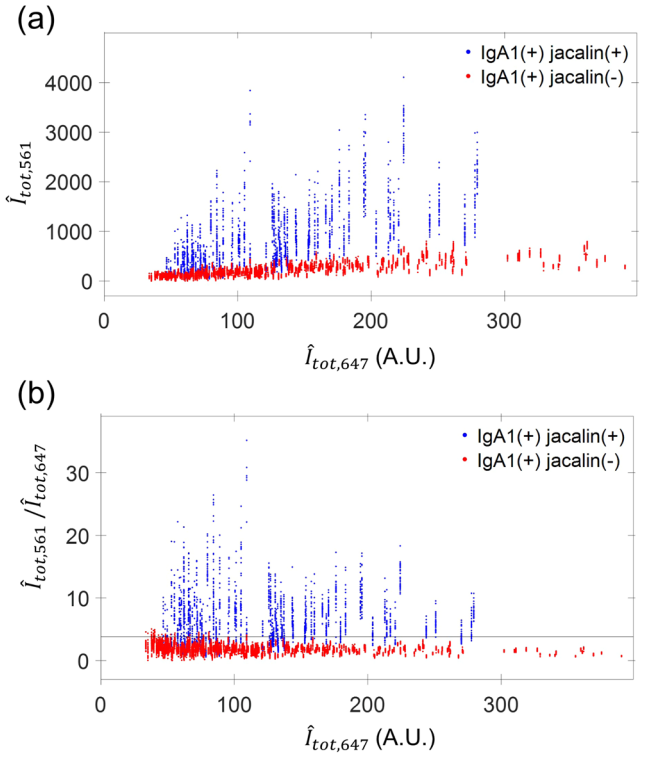

Figure 2. (a) The particle brightness in the FRET channel $I_{tot,561}$ plotted with respect to the particle brightness in the IgA1 channel $I_{tot,647}$. (b) The particle brightness in the FRET channel divided by the brightness of the corresponding particles in the IgA1 channel $I_{tot,561}/I_{tot,647}$ plotted with respect to the particle brightness in the IgA1 channel $I_{tot,647}$. The black line denotes the threshold.

https://doi.org/10.1021/acs.analchem.5c01488
Anal. Chem. 2025, 97, 14388−14396

After removing variability due to acceptor dye number, the brightness intensity is still varying due to the variable number of donor fluorophores on the jacalin molecule and their variable distances from the acceptor fluorophores. The distributions of the brightnesses of individual observations of spots for each experiment showed that an increasing jacalin concentration led to a disproportionate increase in the frequency of very bright events, which is potentially indicative of double binding (Figures S16 and S17).

We defined the threshold intensity ratio separating unoccupied IgA1 molecules from occupied IgA1 molecules as the mean of the control plus 3 standard deviations (Figure 2b).

Since the choice of the threshold is critical, we examined the distribution of brightness ratio values under different conditions more closely (Figure 3). Histograms of the

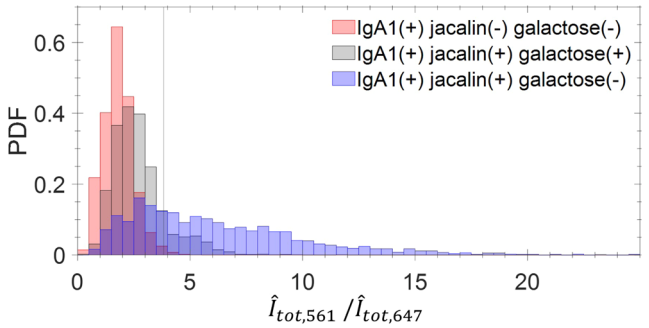

Figure 3. Brightness ratio distribution of all particles in the first 31 frames when jacalin was absent (n = 11,204 measurements, red), when jacalin was present (n = 2643 measurements, blue), and when galactose was added (n = 4497 measurements, gray). The black vertical line represent the threshold used to define on and off events.

observed brightness ratios of the IgA1 sites in the absence of jacalin (signal due to weakly excited IgA1 fluorescence), IgA1 sites in the presence of 800 nM jacalin blocked by 500 mM galactose (signal due to weakly excited IgA1 and nonspecific binding), and IgA1 sites in the presence of 800 nM jacalin (signal due to weakly excited IgA1, nonspecific and specific binding) show that specific binding events can be largely but not completely separated from nonspecific binding events. This is because of many factors that influence the FRET efficiency, such as the interdye distance, dye−dye quenching, and relative orientations of the dipoles of donor and acceptor dyes.[50,51] This is significantly complicated by the fact that the dye-protein ratio differs from IgA1 to IgA1 and different donor and acceptor dyes can photoblink at different rates. Notwithstanding the inevitable overlap between the brightness distributions of specific and nonspecific binding, the chosen threshold represents a suitable compromise.

When a probe concentration of 800 nM jacalin without galactose was applied, a large fraction of the physisorbed IgA1 molecules had a brightness ratio above the threshold indicating the jacalin probe was present, which implies that the dissociation constant is on the order of 1 μM. Out of the IgA1 that remained on the surface after 30 min, 96% of the IgA1 molecules had a jacalin probe present at some point during the 1 h observation window (Table 1), which indicates that the glycan binding sites are accessible for almost all physisorbed IgA1 molecules.

Single IgA1 kinetic data (binding rate, unbinding rate, equilibrium constant) can now be calculated from each time trace (Figure 4). Our calculation of the binding and unbinding

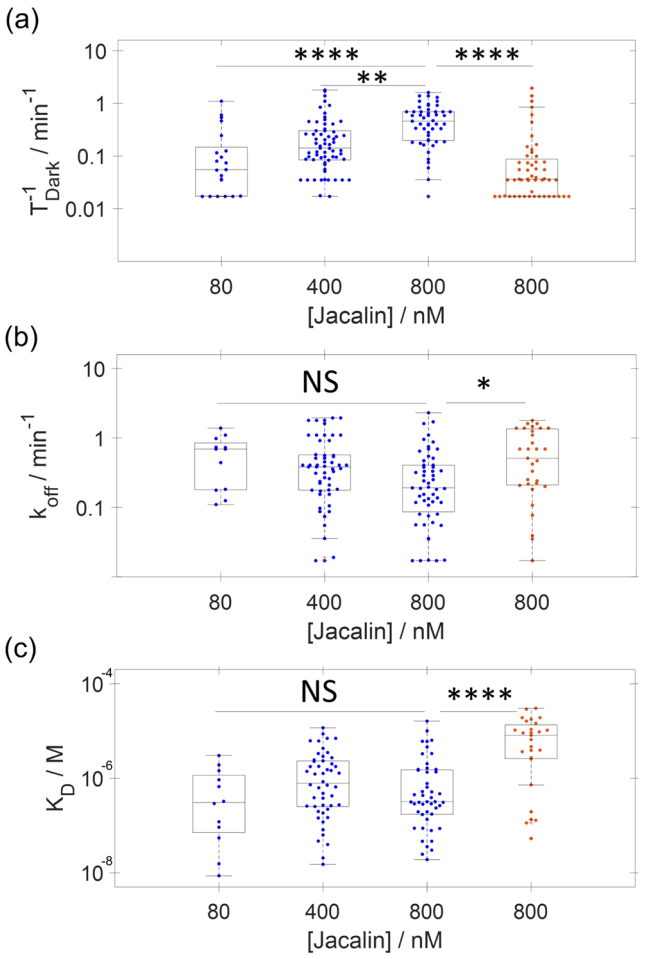

Figure 4. Distribution of (a) binding rates, (b) unbinding rates, and (c) dissociation constants for jacalin binding to single IgA1 particles. Experiment with no galactose added (blue) and control with 500 mM galactose added (orange); box plots represent median and IQR. Error bars denote minimum and maximum values excluding outliers. Statistical difference is calculated with Kruskal−Wallis tests: NS, not significant - $p > 0.05$, * - $P < 0.05$, ** - $P < 0.01$, **** - $P < 0.0001$.

rates utilizes the assumption that a single exponential can describe on and off time distributions. While this is not typically the case for single molecule experiments,[48,52,53] a single exponential model is preferred over a double exponential model due to the small number of observed transitions (Figures S23−S24), in line with the framework of the Akaike Information Criterion.[54] The dynamic range of the rate determination is limited by the number of images acquired (61) to 2−3 orders of magnitude. The individual binding and unbinding rates are distributed around the median values so that approximately 50% of the observations fall within a range of a factor of 10. The individual K_D values are distributed around the median values such that 50% of the observations fall within a factor of 30−100 (as expected based on the individual rates). This implies that the activation energies for binding and unbinding of jacalin to the surface-adhered IgA1 vary within a range of 2−3 k_BT, which is not an implausible result for physisorbed IgA1.

https://doi.org/10.1021/acs.analchem.5c01488
Anal. Chem. 2025, 97, 14388−14396

Similar to ensemble measurements from surface plasmon resonance (SPR) experiments, multiple rates of binding were observed. While fitting of the SPR data could not consider the molecule-to-molecule variability, our single molecule measurements fall within an order of magnitude of the pairs of rates from the fits to the SPR data (Figures S21 and 22, and table S2).

While others have studied the heterogeneity of proteins randomly physisorbed to a surface or covalently linked to a surface, the distribution of individual binding rates, unbinding rates, and dissociation constants often has not been shown, presumably due to the low signal-to-noise ratio in most single molecule experiments. A popular method of assessing the heterogeneity of affinities of a probe in solution to a protein adsorbed to a surface is fitting the data to the Sips isotherm with a variable heterogeneity coefficient.[55,56] Vijayendran et al. used this method to show that the heterogeneity of trinitrobenzene in solution binding to anti-TNT antibodies on a surface is significantly larger when the antibodies are immobilized in random conformations than when they are tethered to the surface by the Fc region.[55] They do not measure the distribution of the rates for individual antibodies, however. Svitel, Gorshkova, and co-workers developed mathematical methods to estimate the spread of the distribution of affinities of probes to proteins on a SPR (surface plasmon resonance) surface using specific sets of assumptions and constraints.[57−60] Depending on the conditions, the individual unbinding rates were distributed such that approximately 50% of the observations fell within a factor of 1.5−10; and the individual K_D values were distributed such that approximately 50% of the observations fell within a factor of 3−100.[57] Temirov et al. covalently attached antibodies to a surface and directly measured the affinity of quantum-dot labeled antigens binding from solution via fluorescence microscopy, and observed that the K_D values were distributed such that approximately 50% of the observations fell within a factor of 3.[61]

Even though our antibodies were physisorbed in random configurations to the surface, the variability of 1 order of magnitude for 50% of the binding and unbinding rates and 2 orders of magnitude for dissociation constants matches the variability observed by Svitel et al. for binding to proteins covalently linked to a surface.[57−59] A more sophisticated immobilization approach may reduce the variability between individual IgA1 to the low level of variability (2-fold) observed for DNA binding to biotinylated DNA immobilized on a streptavidin layer on a PEG layer.[62] However, the variability may simply reflect the uncertainty of each individual measurement, which is around one order of magnitude (Figures S6−S8). Reassuringly, our final measured dissociation constant for jacalin and IgA1 based on the average unbinding rate divided by the slope of a linear regression fit of the binding rates of 0.8 μM, is close to the published value from an ensemble measurement of the association constant of 0.80 ± 0.09 $(\mu M)^{-1}$ which is equivalent to a dissociation constant of 1.3 μM.[63]

Monte Carlo simulations were conducted to check that the specific binding with optimized rates in the presence of noise, nonspecific binding, and overlapping binding events yield relative brightness traces similar to the experimental data. The simulations modeled three possible states for specific binding: dark, single-binding, and double binding (since IgA1 molecules have two hinges); and two possible states of nonspecific binding: dark and bright. First, it was assumed that the brightness distribution in the dark state, which could be attributed to the direct excitation of the multiple acceptor dyes on an IgA1, was Gaussian-distributed. Second, it was assumed that the observable brightness distribution for both specific single-binding and nonspecific binding are independently Gaussian distributed, and that the means and variance for specific double binding are double those of single-binding. Finally, it was assumed that the observed brightness was the sum of three contributions: the brightness in the dark state, the brightness due to nonspecific binding, and the brightness due to specific binding. The three distributions' parameters were calculated based on the brightness distributions of the experiment with jacalin present, the control without jacalin present, and the control with both jacalin and galactose competitor present (Figures 3 and S13; see Supporting Information). The brightness distribution parameters were then fixed so that the kinetic rates from the simulation could be optimized and compared to the kinetic rates of the experiment (Figures S18 and S19).

For the simulations to reproduce the experimentally observed brightness distribution when specific binding was inhibited by galactose (Figures 3 and S14), nonspecific binding was allowed. Nonspecific on and off rates were estimated to be 0.29 $(\mu M\ min)^{-1}$ and 0.083 min^{-1} respectively. These parameters, when used in simulations without specific binding included, successfully reproduced the experimental brightness distribution in the presence of 500 mM galactose (Figure S14). After specific binding was added to the simulations, simulations reproduced the experimentally observed shift in the brightness distribution toward higher brightness values when double binding is included (Figures S16 and S17). Finally, the simulations reproduce the decrease of the unbinding rate with increasing jacalin concentration, which originates in overlapping binding events from both specific and nonspecific binding (Figure 5). This overlapping makes events appear longer than they truly are. The optimized specific on and off rates are 0.45 $(\mu M\ min)^{-1}$ and 0.3 min^{-1}, respectively.

The simulations also highlighted how the detection threshold affects the observed kinetics of the dim nonspecific binding events. The observed binding rates decrease when galactose is introduced (Figure 4a) as expected if jacalin binds specifically to glycans on IgA1. The remaining binding rate is due to nonspecific binding, which occurs at a lower but not insignificant rate. However, the observed unbinding rates increase when galactose is present (Figure 4b) because nonspecifically bound jacalin molecules are likely to randomly drop below the threshold and thereby give the impression of unbinding. This dynamic is captured in the simulations where nonspecific binding events emerge as being longer in duration than specific binding events, similar to the observations of Chatterjee et. al.[19]

CONCLUSIONS

Our experiments demonstrated that FRET is sufficient to suppress the elevated background from a high jacalin solution concentration and nonspecific binding to the surface. This allows us to observe binding of low on-rate jacalin probes and can be exploited in other single molecule experiments with protein probes.

Significant variability between the affinity of individual IgA1 for jacalin binding is found, with binding affinities of jacalin to single IgA1 molecules varying by several orders of magnitude.

https://doi.org/10.1021/acs.analchem.5c01488
Anal. Chem. 2025, 97, 14388−14396

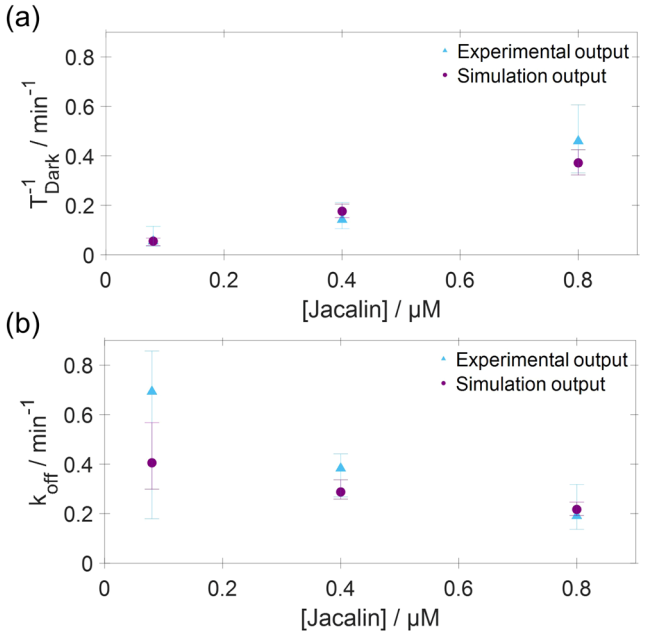

Figure 5. Median kinetic rates of jacalin binding to IgA1. (a) The median of the binding rates for each IgA1 molecule (τ_{dark}^{-1}) with 95% confidence intervals from bootstrapping at different jacalin concentrations compared to the median from 300 simulations with 95% confidence intervals. (b) The median of the unbinding rates for each IgA1 molecule (k_{off}) with 95% confidence intervals from bootstrapping at different jacalin concentrations compared to the median from 300 simulations with 95% confidence intervals.

For between 4 and 50% of the IgA1 we do not observe any binding events and for another 0 to 24% of the IgA1 we do not observe any unbinding events from an initially bright state. This may partially reflect the dynamic range of our method and partially the absence or inaccessibility on glycans on these IgA1, as well as irreversible binding events e.g., due to photoinduced cross-linking.[64] Jacalin binding may be further influenced by varying IgA1 conformational changes and varying IgA1 adsorption geometries, which can be caused by varying microenvironments on a glass surface.[65,66] The effects of surface heterogeneities and electrostatic interactions on local pH and IgA1 are complex. For example, Aggarwal et al. observed that bovine serum albumin binding to a hybrid surface made of silica and zirconia cannot be accounted for by the binding to each independently; they suggest that adsorbing bovine serum albumin's surface can interact with heterogeneities on the substrate, leading to unexpected results.[67] Additionally, Cai et al. observe that even on fused-silica glass surfaces, specific sites exhibited anomalously strong binding, likely due to varying numbers and arrangements of silanol and siloxane groups on the glass.[68] Another possible source of binding heterogeneity is probe heterogeneity, which can be caused by probe oligomerization, probe denaturization, or differences in steric hindrance due to differing dye protein ratios. For example, Langdon et al. observed that oligomers bind to polymer films longer than monomers.[69] Despite the variability in affinity of individual IgA1 arising from all these contributions, the binding affinities in the presence and absence of galactose are highly significantly different (Figure 4c), and individual affinity measurements can be assigned to specific or nonspecific binding with some confidence.

The dynamic range of the measurement method is determined by the number of acquired images. The number of acquired frames is not primarily limited by photobleaching, because IgA1 molecules are only imaged every 30 min and jacalin molecules are only imaged for the duration of one binding event. Instead, the overall length of the experiment is limited to roughly 10 h by the detachment of IgA1 from the surface, an accumulation of nonspecifically bound jacalin and the exhaustion of the oxygen scavenging system. The frequency of imaging has to be sufficiently high to allow the determination of the fastest unbinding rate, that is it should be at least 2-fold higher. To make full use of the dynamic range for the determination of the binding rate, the solution concentration of the probe should be adjusted so that binding rates match unbinding rates. We chose an imaging frequency of 1 per minute where transitions have a relatively high probability. This spacing between images, however, makes many dark and bright events truncated, as the length of a binding event shorter than a minute cannot be measured. A comprehensive analysis method for the truncated data was developed in which instead of considering length of events, the changes in state between individual frames is used to calculate binding and unbinding times. Based on the Wilson confidence interval for proportions of populations, the 95% confidence intervals for the kinetic rates were determined to be 1 order of magnitude wide (Figures S6−S8). The trade-offs between the error of individual measurements (determined by the number of events observed), the range of detectable values (determined by the time between frames and the time between the first and last frame), and the confidence in individual measurements (determined by the signal strength resulting from the exposure time) are complex and have to be carefully considered.

Nonspecific binding of the jacalin probes to the surface was still a factor in our measurements, even though the employed blocking reagent reduced adsorption 20-fold (Figure S1). While better surface coatings exist,[37] we found that more complex surface modification leads to an increased number of fluorescent objects on the surface. Our approach was to eliminate the signal from nonspecifically bound probes based on their fluorescence intensity.

The fluorescence intensity of the FRET signal is inherently variable, due to variability in the number of fluorophores on each target and probe when primary amines are labeled. This increases the width of the brightness distribution of the FRET signal. This effect is amplified by the blinking of fluorescent dyes, which we suppressed by adding triplet quenchers. New dyes with less photoblinking[70,71] (e.g., Janelia fluor dyes) and further optimization of the triplet quenchers offer room for further improvement.

Despite these challenges, the sensitivity of the assay is sufficient to detect the presence of O-linked glycans on IgA1. The number of jacalin binding sites can range from 1 to 10 given that jacalin binding glycans may be present on one or all of the 5 primary glycosylation sites on each hinge. Since we can observe only on the order of 100 binding events for each IgA1, the exact number of jacalin binding sites cannot be determined from the on-rate due to stochastic variations. Our analysis of the intensity of the FRET signal showed evidence of double binding of jacalin to the same IgA1 suggesting that the intensity may be an additional parameter to identify distinct IgA1 populations. Our future work will determine whether we

https://doi.org/10.1021/acs.analchem.5c01488
Anal. Chem. 2025, 97, 14388−14396

can distinguish IgA1 populations from healthy donors and donors with IgA nephropathy.

■ ASSOCIATED CONTENT

Supporting Information

The Supporting Information is available free of charge at https://pubs.acs.org/doi/10.1021/acs.analchem.5c01488.

Surface treatment, image and data analysis, simulation (PDF)

■ AUTHOR INFORMATION

Corresponding Author

Henry Hess − *Department of Biomedical Engineering, Columbia University, New York, New York 10027, United States;* orcid.org/0000-0002-5617-606X; Email: hh2374@columbia.edu

Authors

Joseph R. Rubin − *Department of Biomedical Engineering, Columbia University, New York, New York 10027, United States*

Steven K. Taylor − *Division of Experimental Therapeutics, Department of Medicine, Columbia University, New York, New York 10032, United States;* orcid.org/0000-0002-9810-4531

Sergei Rudchenko − *Division of Experimental Therapeutics, Department of Medicine, Columbia University, New York, New York 10032, United States*

Milan N. Stojanovic − *Department of Biomedical Engineering, Columbia University, New York, New York 10027, United States; Division of Experimental Therapeutics, Department of Medicine, Columbia University, New York, New York 10032, United States*

Complete contact information is available at: https://pubs.acs.org/10.1021/acs.analchem.5c01488

Author Contributions

M.N.S. and H.H. conceived and designed the research. J.R.R. performed the experiments and analyzed the data with guidance from S.R. and S.K.T.. S.R. did the SPR experiments. All authors discussed the results and contributed to editing the manuscript.

Notes

The authors declare no competing financial interest.

■ ACKNOWLEDGMENTS

We gratefully acknowledge Dr. Ali Gharavi's guidance in defining the clinical needs, and Dr. Sergei Rudchenko, Dr. Meghana Shamsunder, Dr. Jeffrey Roskes and Dr. Ivan Cohen for helpful discussions. J.R.R. acknowledges support from Columbia University TL1 TR001875 doctoral training program. H.H. and M.N.S. acknowledge support by a Columbia University RISE award and R21HG012543.

■ REFERENCES

(1) Donadio, J. V.; Grande, J. P. *N. Engl. J. Med.* **2002**, *347* (10), 738−749.

(2) Suzuki, H.; Kiryluk, K.; Novak, J.; Moldoveanu, Z.; Herr, A. B.; Renfrow, M. B.; Wyatt, R. J.; Scolari, F.; Mestecky, J.; Gharavi, A. G.; Julian, B. A. *J. Am. Soc. Nephrol.* **2011**, *22* (10), 1795−1803.

(3) Barratt, J.; Feehally, J. *J. Am. Soc. Nephrol.* **2005**, *16* (7), 2088−2097.

(4) Saldova, R.; Wilkinson, H. *J. Proteome Res.* **2020**, *19* (10), 3890−3905.

(5) Lehoux, S.; Ju, T.Separation of Two Distinct O-Glycoforms of Human IgA1 by Serial Lectin Chromatography Followed by Mass Spectrometry O-Glycan Analysis. In *Methods Enzymology*; Elsevier, 2017; Vol. *585*, pp 61−75.

(6) Takahashi, K.; Smith, A. D.; Poulsen, K.; Kilian, M.; Julian, B. A.; Mestecky, J.; Novak, J.; Renfrow, M. B. *J. Proteome Res.* **2012**, *11* (2), 692−702.

(7) Lelek, M.; Gyparaki, M. T.; Beliu, G.; Schueder, F.; Griffié, J.; Manley, S.; Jungmann, R.; Sauer, M.; Lakadamyali, M.; Zimmer, C. *Nat. Rev. Methods Primers* **2021**, *1* (1), No. 39.

(8) Han, R.; Li, Z.; Fan, Y.; Jiang, Y. *J. Genet. Genomics* **2013**, *40* (12), 583−595.

(9) Betzig, E.; Patterson, G. H.; Sougrat, R.; Lindwasser, O. W.; Olenych, S.; Bonifacino, J. S.; Davidson, M. W.; Lippincott-schwartz, J.; Hess, H. F. *Science* **2006**, *313* (5793), 1642−1645.

(10) Hess, S. T.; Girirajan, T. P. K.; Mason, M. D. *Biophys. J.* **2006**, *91* (11), 4258−4272.

(11) Biteen, J. S.; Thompson, M. A.; Tselentis, N. K.; Bowman, G. R.; Shapiro, L.; Moerner, W. E. *Nat. Methods* **2008**, *5* (11), 947−949.

(12) Lee Upton, S.; Tay, J. W.; Schwartz, D. K.; Sousa, M. C. *Biophys. J.* **2023**, *122* (22), 4382−4394.

(13) Van De Linde, S.; Löschberger, A.; Klein, T.; Heidbreder, M.; Wolter, S.; Heilemann, M.; Sauer, M. *Nat. Protoc.* **2011**, *6* (7), 991−1009.

(14) Wang, F.; Liu, Y.; Cheng, X.; Yin, W. *Front. Chem.* **2021**, *9*, No. 655324.

(15) Jungmann, R.; Steinhauer, C.; Scheible, M.; Kuzyk, A.; Tinnefeld, P.; Simmel, F. C. *Nano Lett.* **2010**, *10* (11), 4756−4761.

(16) Mishra, A.; Behura, A.; Mawatwal, S.; Kumar, A.; Naik, L.; Mohanty, S. S.; Manna, D.; Dokania, P.; Mishra, A.; Patra, S. K.; Dhiman, R. *Food Chem. Toxicol.* **2019**, *134*, No. 110827.

(17) Dai, M.; Jungmann, R.; Yin, P. *Nat. Nanotechnol.* **2016**, *11* (9), 798−807.

(18) Mandal, S.; Li, Z.; Chatterjee, T.; Khanna, K.; Montoya, K.; Dai, L.; Petersen, C.; Li, L.; Tewari, M.; Johnson-Buck, A.; Walter, N. G. *Acc. Chem. Res.* **2021**, *54* (2), 388−402.

(19) Chatterjee, T.; Knappik, A.; Sandford, E.; Tewari, M.; Choi, S. W.; Strong, W. B.; Thrush, E. P.; Oh, K. J.; Liu, N.; Walter, N. G.; Johnson-Buck, A. *Proc. Natl. Acad. Sci. U.S.A.* **2020**, *117* (37), 22815−22822.

(20) Khanna, K. Rapid Single Molecule FRET Biosensing Assay for Nucleic Acid Detection. Ph.D. Dissertation; University of Michigan2022.

(21) Grönwall, C.; Ståhl, S. *J. Biotechnol.* **2009**, *140* (3−4), 254−269.

(22) Filius, M.; Cui, T. J.; Ananth, A. N.; Docter, M. W.; Hegge, J. W.; Van Der Oost, J.; Joo, C. *Nano Lett.* **2020**, *20* (4), 2264−2270.

(23) Milton, J. D.; Fernig, D. G.; Rhodes, J. M. *Glycoconjugate J.* **2001**, *18* (7), 565−569.

(24) Duverger, E.; Frison, N.; Roche, A. C.; Monsigny, M. *Biochimie* **2003**, *85* (1−2), 167−179.

(25) Lee, J.; Park, S.; Hohng, S. *Mol. Brain* **2018**, *11*, No. 70.

(26) Lerner, E.; Barth, A.; Hendrix, J.; Ambrose, B.; Birkedal, V.; Blanchard, S. C.; Börner, R.; Chung, H. S.; Cordes, T.; Craggs, T. D.; et al. *eLife* **2021**, *10*, 1−69.

(27) Mazal, H.; Haran, G. *Curr. Opin. Biomed. Eng.* **2019**, *12*, 8−17.

(28) Li, C. c.; Li, Y.; Zhang, Y.; Zhang, C. y. *TrAC, Trends Anal. Chem.* **2020**, *122*, No. 115753.

(29) Sasmal, D. K.; Pulido, L. E.; Kasal, S.; Huang, J. *Nanoscale* **2016**, *8* (48), 19928−19944.

(30) Lerner, E.; Cordes, T.; Ingargiola, A.; Alhadid, Y.; Chung, S. Y.; Michalet, X.; Weiss, S. *Science* **2018**, *359* (6373), No. eaan1133, DOI: 10.1126/science.aan1133.

(31) Qiao, Y.; Luo, Y.; Long, N.; Xing, Y.; Tu, J. *Micromachines* **2021**, *12* (5), No. 492.

(32) Kienle, D. F.; Schwartz, D. K. *Anal. Chim. Acta* **2021**, *1154*, No. 338331.

(33) Leckband, D.; Schwartz, D. K.; Wu, Y. *Biophys. J.* **2024**, *123* (4), 424−434.
(34) Benítez, J. J.; Keller, A. M.; Chen, P.Nanovesicle Trapping for Studying Weak Protein Interactions by Single-molecule FRET. In *Methods in Enzymology*; Elsevier, 2010; Vol. *472*, pp 41−60.
(35) Benítez, J. J.; Keller, A. M.; Ochieng, P.; Yatsunyk, L. A.; Huffman, D. L.; Rosenzweig, A. C.; Chen, P. *J. Am. Chem. Soc.* **2008**, *130* (8), 2446−2447.
(36) Filius, M.; van Wee, R.; de Lannoy, C.; Westerlaken, I.; Li, Z.; Kim, S. H.; de Agrela Pinto, C.; Wu, Y.; Boons, G. J.; Pabst, M.; et al. *Nat. Nanotechnol.* **2024**, *19* (5), 652−659.
(37) Katira, P.; Agarwal, A.; Fischer, T.; Chen, H. Y.; Jiang, X.; Lahann, J.; Hess, H. *Adv. Mater.* **2007**, *19* (20), 3171−3176.
(38) Katira, P.; Agarwal, A.; Hess, H. *Adv. Mater.* **2009**, *21* (16), 1599−1604.
(39) Hucknall, A.; Rangarajan, S.; Chilkoti, A. *Adv. Mater.* **2009**, *21* (23), 2441−2446.
(40) Chatterjee, T.; Johnson-Buck, A.; Walter, N. G. *Biosens. Bioelectron.* **2022**, *216*, No. 114639.
(41) Sanders, E. W.; Carr, A. R.; Bruggeman, E.; Körbel, M.; Benaissa, S. I.; Donat, R. F.; Santos, A. M.; McColl, J.; O'Holleran, K.; Klenerman, D.; et al. *Angew. Chem.* **2022**, *134* (42), No. e202206919.
(42) Smith, E. A.; Thomas, W. D.; Kiessling, L. L.; Corn, R. M. *J. Am. Chem. Soc.* **2003**, *125* (20), 6140−6148.
(43) Hagiwara, K.; Collet-Cassart, D.; Kunihiko, K.; Vaerman, J. P. *Mol. Immunol.* **1988**, *25* (1), 69−83.
(44) Sako, Y.; Minoghchi, S.; Yanagida, T. *Nat. Cell Biol.* **2000**, *2* (3), 168−172.
(45) Ušaj, M.; Moretto, L.; Vemula, V.; Salhotra, A.; Månsson, A. *Commun. Biol.* **2021**, *4* (1), No. 64.
(46) Schindelin, J.; Arganda-Carreras, I.; Frise, E.; Kaynig, V.; Longair, M.; Pietzsch, T.; Preibisch, S.; Rueden, C.; Saalfeld, S.; Schmid, B.; et al. *Nat. Methods* **2012**, *9* (7), 676−682.
(47) Schnitzbauer, J.; Strauss, M. T.; Schlichthaerle, T.; Schueder, F.; Jungmann, R. *Nat. Protoc.* **2017**, *12* (6), 1198−1228.
(48) Kastantin, M.; Langdon, B. B.; Chang, E. L.; Schwartz, D. K. *J. Am. Chem. Soc.* **2011**, *133* (13), 4975−4983.
(49) Violin Plots for Plotting Multiple Distributions (distributionPlot.m); MATLAB Central File Exchange. https://www.mathworks.com/matlabcentral/fileexchange/23661-violin-plots-for-plotting-multiple-distributions-distributionplot-m. (accessed May 28, 2025).
(50) Di Fiori, N.; Meller, A. *Biophys. J.* **2010**, *98* (10), 2265−2272.
(51) Nir, E.; Michalet, X.; Hamadani, K. M.; Laurence, T. A.; Neuhauser, D.; Kovchegov, Y.; Weiss, S. *J. Phys. Chem. B* **2006**, *110* (44), 22103−22124.
(52) Poongavanam, M. V.; Kisley, L.; Kourentzi, K.; Landes, C. F.; Willson, R. C. *Biochim. Biophys. Acta, Proteins Proteomics* **2016**, *1864* (1), 154−164.
(53) Armstrong, M. J.; Rodriguez, J. B.; Dahl, P.; Salamon, P.; Hess, H.; Katira, P. *Langmuir* **2020**, *36* (45), 13527−13534.
(54) Akaike, H. *IEEE Trans. Autom. Control* **1974**, *19* (6), 716−723.
(55) Vijayendran, R. A.; Leckband, D. E. *Anal. Chem.* **2001**, *73* (3), 471−480.
(56) Ibii, T.; Kaieda, M.; Hatakeyama, S.; Shiotsuka, H.; Watanabe, H.; Umetsu, M.; Kumagai, I.; Imamura, T. *Anal. Chem.* **2010**, *82* (10), 4229−4235.
(57) Gorshkova, I. I.; Svitel, J.; Razjouyan, F.; Schuck, P. *Langmuir* **2008**, *24* (20), 11577−11586.
(58) Zhao, H.; Gorshkova, I. I.; Fu, G. L.; Schuck, P. *Methods* **2013**, *59* (3), 328−335.
(59) Svitel, J.; Balbo, A.; Mariuzza, R. A.; Gonzales, N. R.; Schuck, P. *Biophys. J.* **2003**, *84* (6), 4062−4077.
(60) Svitel, J.; Boukari, H.; Van Ryk, D.; et al. *Biophys. J.* **2007**, *92* (5), 1742−1758.
(61) Temirov, J. P.; Bradbury, A. R. M.; Werner, J. H. *Anal. Chem.* **2008**, *80* (22), 8642−8648.
(62) Elenko, M. P.; Szostak, J. W.; Van Oijen, A. M. *Rev. Sci. Instrum.* **2010**, *81*, No. 083705.
(63) Pedroso, M. M.; Pesquero, N. C.; Thomaz, S. M.; Roque-Barreira, M. C.; Faria, R. C.; Bueno, P. R. *Glycobiology* **2012**, *22* (3), 326−331.
(64) Yan, P.; Xiong, Y.; Chen, B.; Negash, S.; Squier, T. C.; Mayer, M. U. *Biochemistry* **2006**, *45* (15), 4736−4748.
(65) Mabry, J. N.; Kastantin, M.; Schwartz, D. K. *ACS Nano* **2015**, *9* (7), 7237−7247.
(66) Bisirri, E. A.; Kaar, J. L.; Schwartz, D. K. *Langmuir* **2025**, *41* (8), 5335−5346.
(67) Aggarwal, N.; Lawson, K.; Kershaw, M.; Horvath, R.; Ramsden, J. *Appl. Phys. Lett.* **2009**, *94*, No. 083110.
(68) Cai, Y.; Schwartz, D. K. *ACS Appl. Mater. Interfaces* **2016**, *8* (1), 511−520.
(69) Langdon, B. B.; Mirhossaini, R. B.; Mabry, J. N.; Sriram, I.; Lajmi, A.; Zhang, Y.; Rojas, O. J.; Schwartz, D. K. *ACS Appl. Mater. Interfaces* **2015**, *7* (6), 3607−3617.
(70) Menzel, R.; Thiel, E. *Chem. Phys. Lett.* **1998**, *291* (1−2), 237−243.
(71) Grimm, J. B.; Tkachuk, A. N.; Xie, L.; Choi, H.; Mohar, B.; Falco, N.; Schaefer, K.; Patel, R.; Zheng, Q.; Liu, Z.; et al. *Nat. Methods* **2020**, *17* (8), 815−821.

https://doi.org/10.1021/acs.analchem.5c01488
Anal. Chem. 2025, 97, 14388−14396